7th International Conference on Fluid Mechanics, ICFM7

A numerical investigation of the dynamic wetting transition on a moving substrate

Ao Liu[a]

[a]*Department of Modern Mechanics, University of Science and Technology of China, Hefei, Anhui, 230026, China*

Abstract

The dynamic wetting transition of an interface on a partially wetting substrate is numerically investigated using a diffuse-interface method. Both advancing and receding contact lines are considered. As the driving speed of the substrate exceeds a threshold, the contact line keeps moving with the plate and cannot remain stable. For the receding case, the onset of wetting transition is found to agree with previous lubrication theory, and the transition can be delayed by changing boundary conditions such that the macroscopic meniscus can maintain a pressure difference. For the transition of an advancing contact line, the apparent contact angle remains finite, and the critical speed decreases with the contact angle, which is opposite to the receding case.
Keywords: moving contact line, contact angle, wetting transition

1. Introduction

It is well known that a three-phase contact line moving relative to a solid wall cannot exceed a maximum speed, beyond which the receding phase of the fluid will be entrained, leading to the formation of liquid films or gas layers [1,2]. The forced wetting or dewetting is an important phenomenon of many environmental and industrial flows, such as the deposition of the pesticides on the plant leaves, the motion of the droplet on the window, painting, coating and oil recovery [3,4]. It is crucial to know when the wetting or dewetting will occur and what will happen after it occurs. This process of dynamic wetting transition is determined primarily by the competition between viscous and capillary forces, measured by the capillary number $Ca = \mu U/\sigma$, where μ is the viscosity of the liquid phase, U is the speed of the contact line and σ is the surface tension [5,6]. Recent work have shown that the onset of wetting transition is influenced by both microscopic flow in the vicinity of the contact line and macroscopic flow away from it [7,8]. However, quantitative analyses are only available for limited geometry configurations.

The dynamics of moving contact line cannot be fully described by hydrodynamics, since the viscous dissipation in the liquid wedge is logarithmically infinite if the no-slip boundary condition is applied at the solid surface [9,10]. This singularity should be circumvented by introducing various contact-line models characterized by the presence of small

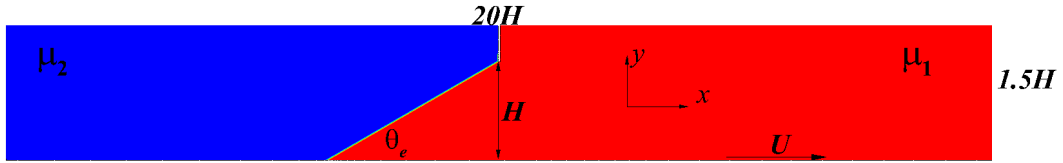*E-mail address:* liuaolow@mail.ustc.edu.cn

Fig. 1. Schematic diagram showing two-phase fluid separated by an interface on a substrate. The upper contact line is pinned by a post and the lower is located at the plate moving with speed U. Initially, the interface is simplify a straight line with a slope determined by the contact angle θ_e.

scales, typically at molecular scale. Therefore, the evolvement of a wide range of length scales leads to considerable challenges in understanding this problem.

The receding contact line has been studied in a lot of work, both theoretically and experimentally, in the last few years. Because of the multiscale characteristic of the wetting flows, the viscosity mainly dominates the flows near the contact line such that the microscopic and macroscopic flows can be considered separately and then matched together through the matched asymptotic expansions [7,11]. This procedure can be easily used to predict the onset of wetting transition in various geometries [11–13]. However, the advancing contact line is much more difficult to understand as the gas plays an important role and makes the problem more confused. Some preliminary works have been carried out to reveal the mechanism of the transition in the situation of the advancing contact line [14–16].

In this work, we study numerically the dynamic wetting transition when a contact line is forced to move over a substrate of arbitrary wettability, for both receding and advancing processes. The purpose is to provide a numerical verification of the criteria for wetting transition and to quantify the influence of the macroscopic meniscus, for the receding case. In addition, the transition of the advancing contact line is considered, focusing on the interfacial profile and the influence of the contact angle.

2. Numerical Method

The problem considered is illustrated in Fig. 1, where two-phase fluids, e.g. liquid and gas, are laid on a substrate moving with a speed U. The viscosities of liquid and gas are μ_1 and μ_2, respectively. For simplicity, the upper contact line is pinned at the end of a post and we focus on the lower contact line. Here, the air and the liquid are separated by an interface with surface tension σ, and both phases are assumed to be incompressible and Newtonian. Inertia effect is ignored owing to the low speed [17,18]. We use a two-dimensional frame of reference with the x- and y-axis coincide with the horizontal plate and the vertical post, respectively.

The diffuse-interface model was used to capture the evolution of the interface [19–21]. A phase-field variable ϕ is introduced to distinguish the two-phase fluids, where $\phi = 1$ in the liquid and $\phi = -1$ in the gas. The evolution of ϕ is governed by the Cahn-Hillard equation:

$$\frac{\partial \phi}{\partial t} + \mathbf{v} \cdot \nabla \phi = \gamma \nabla^2 G. \tag{1}$$

where $G = \lambda[-\nabla^2 \phi + (\phi^2 - 1)\phi/\epsilon^2]$ is the bulk chemical potential, γ is the mobility and $\mathbf{v} = (u, v)$ is the velocity vector. λ is the mixing energy density and ϵ is the capillary width characterizing the thickness of the diffuse interface; they are related to the surface tension σ by $\sigma = 2\sqrt{2}\lambda/3\epsilon$ [21]. The flow is governed by the Stokes equations:

$$\nabla \cdot \mathbf{v} = 0, \tag{2}$$

$$-\nabla p + \mu \nabla \mathbf{v}^2 + G \nabla \phi = 0, \tag{3}$$

where $\mu = [(1 + \phi)\mu_1 + (1 - \phi)\mu_2]/2$.

The bottom boundary is a solid wall with a horizontal speed $\pm U$, with "+" and "−" denoting the advancing and receding contact line, respectively. For all calculations, the no-slip and no-penetration boundary conditions are applied at the bottom wall and the post. The contact angle θ_e can be specified by a boundary condition for ϕ [19]. Two different groups of conditions are used at the remaining boundaries. In the first model, we use open-boundary conditions with stress free elsewhere. In the second model, a stationary wall is introduced at the upper boundary, and a zero-flux
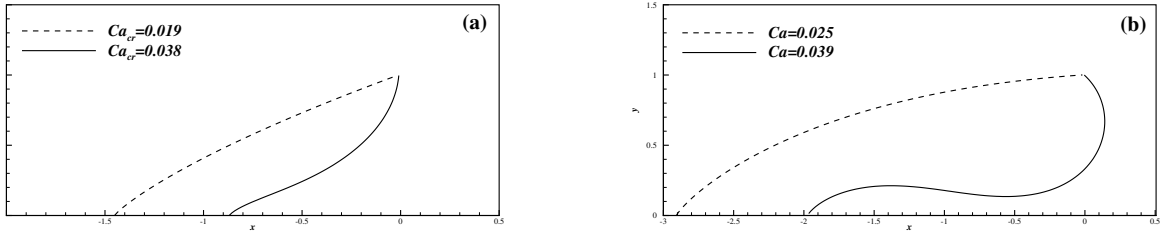
Fig. 2. Interfacial profiles when (a) $Ca = Ca_{cr}$ and (b) $Ca > Ca_{cr}$ for receding contact lines. The latter is unsteady and only instantaneous interfaces are shown. The solid and dash lines denote zero-flux and open-boundary conditions, respectively. The contact angle is $\theta_e = 60°$.
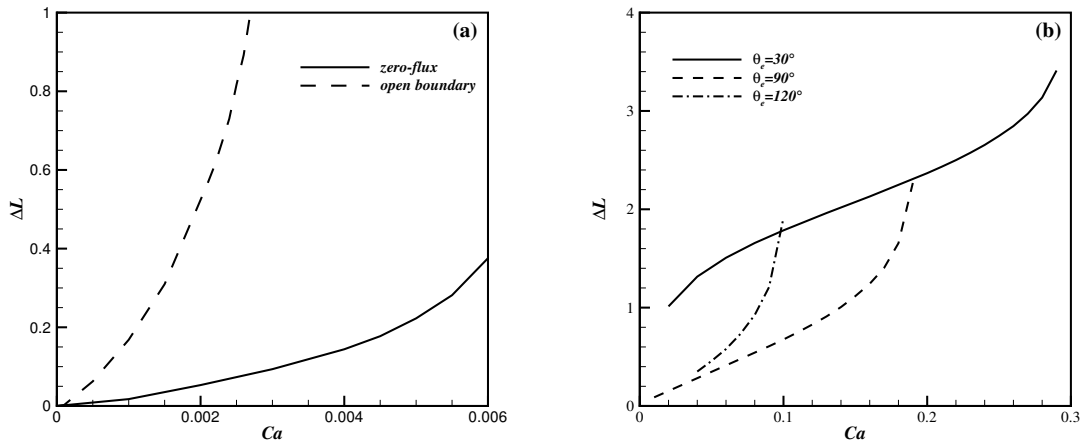

Fig. 3. (*a*) Variation of the contact-line displacement, ΔL, with Ca for $\theta_e = 30°$. (*b*) Same as (*a*) but for advancing contact lines with different contact angles.

condition is imposed at the left and right boundaries. The second boundary condition will only be used in section 3.1 as a comparison for the case of receding contact line.

The computational domain is $20H \times 1.5H$ with a post of $0.02H \times 0.5H$ in the middle, where H is the distance between the tip of the post and the lower substrate. The governing dimensionless number is the capillary number $Ca = \mu_1 U / \sigma$, which measures the balance between the viscous force and surface tension. We set the viscosity ratio $\mu_1 / \mu_2 = 50$. In the diffuse-interface method, two additional dimensionless parameters are involved: the Cahn number $Cn = \epsilon / H = 0.01$ and $S = \sqrt{\gamma \mu^*} / H = 0.01$, where $\mu^* = \sqrt{\mu_1 \mu_2}$. These values satisfy the criteria $Cn < 4S$ for the convergence to the sharp-interface limit [22].

3. Results and Discussion

3.1. Receding contact line

For both of the two models with different boundary conditions, our numerical results show that the interface evolves toward a new equilibrium state when Ca is smaller than a critical value Ca_{cr}. A further increase of Ca leads to the entrainment of the liquid over the lower substrate. Fig. 2(a) illustrates the interfacial profiles when $Ca = Ca_{cr}$, which exhibit remarkably different features. First, the displacement of the contact line for the stress-free condition is larger than that for non-flux condition. Second, the macroscopic menisci show curvatures with opposite signs; the meniscus
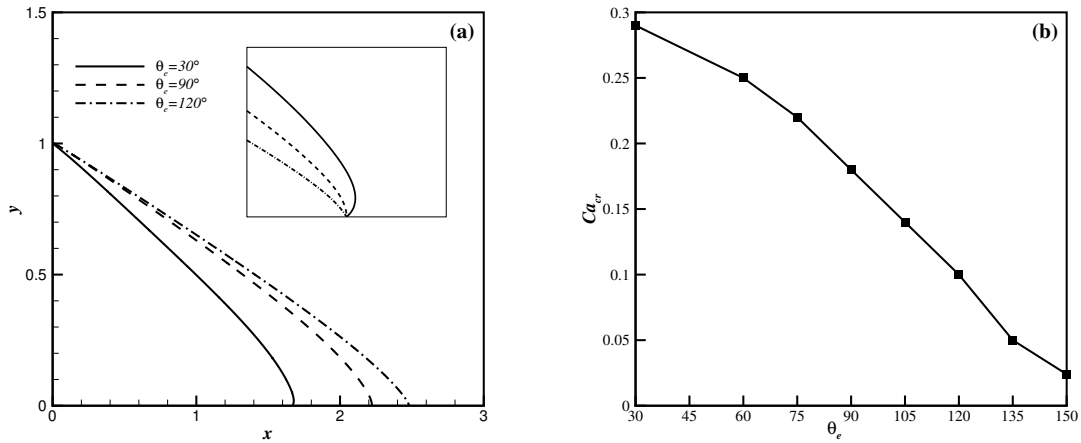
Fig. 4. (*a*) The shape of meniscus with different contact angles when $Ca = Ca_{cr}$. Inset: The meniscus shape near the contact line with different contact angle. (*b*) Variation of Ca_{cr} for the advancing contact line as a function of θ_e.

for the stress-free (no-flux) condition has a convex (concave) shape. Fig. 2(b) shows typical interfacial profiles when film deposition occurs. Since the contact line keeps moving toward the left, only instantaneous interfaces are plotted. It is seen that the thickness of the deposited film for the stress-free condition is $O(1)$ in dimensionless form, while that for the no-flux condition is much thinner.

To quantify the interfacial deformation induced by the moving substrate as well as the onset of film deposition, Fig. 3(a) plots the displacement of the contact line, ΔL, as a function of Ca for $\theta_e = 30°$. It is seen that the contact-line displacement can be significantly suppressed by the no-flux constraint, and the dynamic wetting transition is significantly delayed as well. The critical capillary number is identified as $Ca_{cr} = 2.9 \times 10^{-3}$ and 6.1×10^{-3} for the stress-free and no-flux conditions, respectively. Interestingly, in the framework of lubrication theory, we can derive an approximate expression of Ca_{cr} for the no-flux case,

$$Ca_{cr} = \frac{\theta_e^3}{9} \ln \left(\frac{RCa_{cr}^{1/3}\theta_e}{18^{1/3}\lambda\pi Ai_{max}^2} \right)^{-1}, \tag{4}$$

following a procedure in Refs. [7,11]. Here, R is the radius of the macroscopic meniscus, which can be approximated as an arc since Ca is small; Ai_{max} is the maximum of the Airy function, and λ is a slip length to regularize the contact line, a counterpart of the diffusion length S in our simulations. With $\theta_e = 30°$ and $\lambda = 0.01$, we obtain $Ca_{cr} = 5.7 \times 10^{-3}$, which is close to the numerical result. Since this formula is derived under the condition that the apparent contact angle vanishes, Our simulation also verifies that the apparent contact angle, which can be obtained by extrapolating the macroscopic meniscus toward the contact line, vanishes at the threshold.

The delay of dynamic wetting transition for the no-flux condition is a manifestation of the fact that the critical condition depends on both the microscopic flow close to the contact line and the macroscopic flow far from it, as indicated by Eq. (4). For the stress-free case, however, the macroscopic meniscus is characterized by a much smaller curvature due to the lack of a significant pressure difference across the interface, leading to a transition at small Ca. On the contrary, the no-flux condition is accompanied by the presence of a large curvature of the interface, as shown in Fig. 2(a), and a stable interface can be maintained even at larger Ca.

3.2. Advancing contact line

The case of advancing contact line is more complicated as the gas phase comes into play, different from the receding case in which the gas can be neglected. The dynamic wetting transition will alternatively leads to the deposition of

a gas layer rather than a liquid film. Fig. 3(b) shows the variation of ΔL with Ca for representative values of the contact angle. Compared with the receding case, the deformation of the interface requires much faster movement of the substrate, corresponding to larger values of Ca. Taking $\theta_e = 30°$ as an example, the critical capillary number $Ca_{cr} = 0.29$ as compared to 0.0029 for the receding case. This is owing to the small viscosity of the gas, which should be supplemented by a large velocity for the viscous force to overwhelm the surface tension. Representative interfacial profiles are shown in Fig. 4(a). It is seen that the interfaces are highly bent near the contact line (see the inset) and almost straight far from it. The inclination angle of the straight part of the interface with respect to the substrate can be defined as the apparent contact angle, which is obviously finite even at the transition. Variation of C_{cr} as a function of θ_e is shown in Fig. 4(b), which exhibits a monotonically decreasing behavior. This is quite different from the critical capillary number of the receding case, which is known to scale as θ_e^3.

4. Summary

We have numerically studied the wetting transition for receding or advancing contact lines. For a receding contact line, the employment of no-flux condition can significantly delay the wetting transition, as compared with the stress-free condition, indicating the important role of the curvature of the macroscopic meniscus; the apparent contact angle for no-flux condition vanishes at the onset of transition, in agreement with available lubrication theory. For the advancing case, the interfaces far from the contact line varies linearly and the apparent contact angle remains finite. The threshold Ca_{cr} decreases with θ_e, and the underlying mechanism deserves further investigation.

Acknowledgements

References

[1] D. Bonn, J. Eggers, J. Indekeu, J. Meunier, E. Rolley, Wetting and spreading, Rev. Mod. Phys. 81 (2009) 739–805.
[2] J. H. Snoeijer, B. Andreotti, Moving contact lines: Scales, regimes, and dynamical transitions, Annu. Rev. Fluid Mech. 45 (2013) 269–292.
[3] D. Qur, Fluid coating on a fiber, Annu. Rev. Fluid Mech. 31 (1999) 347–384.
[4] S. J. Weinstein, K. J. Ruschak, Coating flows, Annu. Rev. Fluid Mech. 36 (2004) 29–53.
[5] O. V. Voinov, Hydrodynamics of wetting, Fluid Dynam. 11 (1977) 714–721.
[6] R. G. Cox, The dynamics of the spreading of liquids on a solid-surface .1. viscous-flow, J. Fluid Mech. 168 (1986) 169–194.
[7] J. Eggers, Hydrodynamic theory of forced dewetting, Phys. Rev. Lett. 93 (2004) 094502.
[8] E. Vandre, M. S. Carvalho, S. Kumar, Delaying the onset of dynamic wetting failure through meniscus confinement, J. Fluid Mech. 707 (2012) 496–520.
[9] C. Huh, L. E. Scriven, Hydrodynamic model of steady movement of a solid/liquid/fluid contact line, J. Colloid Interface Sci. 35 (1971) 85–101.
[10] E. B. Dussan, S. H. Davis, Motion of a fluid-fluid interface along a solid-surface, J. Fluid Mech. 65 (1974) 71–95.
[11] J. Eggers, Existence of receding and advancing contact lines, Phys. Fluids 17 (2005) 082106.
[12] J. H. Snoeijer, J. Eggers, Asymptotic analysis of the dewetting rim, Phys. Rev. E 82 (2010) 056314.
[13] T. S. Chan, T. Gueudre, J. H. Snoeijer, Maximum speed of dewetting on a fiber, Phys. Fluids 23 (2011) 112103.
[14] E. Vandre, M. S. Carvalho, S. Kumar, On the mechanism of wetting failure during fluid displacement along a moving substrate, Phys. Fluids 25 (2013) 102103.
[15] T. S. Chan, S. Srivastava, A. Marchand, B. Andreotti, L. Biferale, F. Toschi, J. H. Snoeijer, Hydrodynamics of air entrainment by moving contact lines, Phys. Fluids 25 (2013) 19.
[16] R. Ledesma-Aguilar, A. Hernandez-Machado, I. Pagonabarraga, Theory of wetting-induced fluid entrainment by advancing contact lines on dry surfaces, Phys. Rev. Lett. 110 (2013) 264502.
[17] J. H. Snoeijer, G. Delon, M. Fermigier, B. Andreotti, Avoided critical behavior in dynamically forced wetting, Phys. Rev. Lett. 96 (2006) 174504.
[18] R. V. Sedev, J. G. Petrov, The critical condition for transition from steady wetting to film entrainment, Colloids Surf. 53 (1991) 147–156.
[19] D. Jacqmin, Contact-line dynamics of a diffuse fluid interface, J. Fluid Mech. 402 (2000) 57–88.
[20] T. Qian, X.-P. Wang, P. Sheng, A variational approach to moving contact line hydrodynamics, J. Fluid Mech. 564 (2006) 333–360.
[21] P. Yue, J. J. Feng, C. Liu, J. I. E. Shen, A diffuse-interface method for simulating two-phase flows of complex fluids, J. Fluid Mech. 515 (2004) 293–317.
[22] P. T. Yue, C. F. Zhou, J. J. Feng, Sharp-interface limit of the Cahn–Hilliard model for moving contact lines, J. Fluid Mech. 645 (2010) 279–294.